ELSEVIER

Catalysis Today 33 (1997) 361–369

CATALYSIS TODAY

Synthesis of high surface area perovskite catalysts by non-conventional routes

A. González [a], E. Martínez Tamayo [a], A. Beltrán Porter [a], V. Cortés Corberán [b,*]

[a] *UIBCM, Dept. de Química Inorgánica, Universidad de Valencia, 46100 Valencia, Spain*
[b] *I. de Catálisis y Petroleoquímica, CSIC, 28049 Madrid, Spain*

Abstract

The use of rare earth-containing perovskite oxides as total oxidation catalysts faces to the difficulty of obtaining high surface area materials and the need of calcination at high temperatures for its synthesis. In this work, perovskite $NdCoO_3$ catalysts with relatively high surface areas were synthesized at soft calcination conditions by two non-conventional routes: heteronuclear organic complexes and amorphous precursors obtained by freeze-drying of nitrates solutions. Depending on the method used, different degrees of homogeneity in the bulk distribution of the component cations, oxygen non-stoichiometry as well as surface Co/Nd atomic ratios are obtained. In this way, the synthetic route determines not only the surface area but also the intrinsic activity per surface unit for total oxidation of hydrocarbons.

Keywords: Neodymium–cobalt perovskite; High-surface-area perovskites; Non-conventional synthesis of oxides; Hydrocarbon catalytic combustion

1. Introduction

Perovskites (ABO_3) and related oxidic materials have focused a great research effort during the last decades. Initially, the interest was due to the broad variety of physical properties these oxides exhibit, such as ferro-, piezo-, and pyroelectricity, magnetism and electrooptical effects. But they also show important chemical features [1]: (i) its crystalline structure can accommodate a wide range of cations (practically all stable elements can enter into it); (ii) cations in the two crystallographic positions can be partially substituted; and (iii) this allow to stabilize a wide range of defect or excess of oxygen, thus stabilizing unstable oxidation states. All these properties have raised their use as structural, refractory, electronic, magnetic and catalytic materials [1–4].

The application of perovskite-type oxides in catalysis was first reported for CO oxidation in 1952 [5]. But the research was boosted by the publication of the paper of Libby [6], who pointed out the potential application of these oxides as automotive exhaust oxidation catalysts. Since then, a great number of works have reported on the catalytic activity of perovskites for different reactions, such as CO and hydrocarbons oxidation and NO_x reduction [7,8], hydrogenation of CO and hydrocarbons [9], total

* Corresponding author. E-mail: vcortes@icp.csic.es.

PII S0920-5861(96)00101-0

oxidation of hydrocarbons and electrochemical reduction of oxygen [10], controlled partial oxidation of hydrocarbons and oxygenated compounds [11], as well as photocatalysis [12].

There is a very high number of natural and synthetic compounds having perovskite structure in which the A and B sites can be occupied by a broad range of metal cations in different oxidation states [13]. Among these compounds, those in which the A position is filled by rare-earth (RE) and the B position by transition metal ions respectively, show a remarkable catalytic activity, which is controlled mostly by the B-site metal, while the effect of RE ion of the A-site is less significative [14–16]. Thus, RE cobaltates and manganates show the highest activity for complete oxidation reactions, regardless of A-site rare-earth ion [17].

However, the use of RE-containing perovskite oxides as combustion catalysts faces to the difficulty of obtaining high surface area materials and the need of calcination at high temperatures for their synthesis. The preparative route plays a critical role on the physical and chemical properties of the reaction products, controlling the structure, morphology, grain size and surface area of the obtained materials [18]. Among the conventional methods, the ceramic method is the more inconvenient as it gives wide grain size distributions, difficult control of homogeneity and needs very high calcination temperatures, which is energy consuming and causes sintering. Coprecipitation is simpler and needs lower calcination temperatures, but suffers from difficulties in stoichiometry control and homogeneity of cationic distribution in the grains. Compared to this, complexation (by citrates, etc.) guarantees stoichiometry and homogeneity of cation distribution, but the big amounts of carbon generated involve the need to increase the calcination temperature. To minimize the above problems is necessary to improve the control of stoichiometry and homogeneity (at both particle and atomic scales) as well as minimize residue to reduce temperature and time of treatment to avoid sintering.

In this work, we investigate non-conventional synthesis routes to perovskites, using $NdCoO_3$ as a model compound, in order to get high surface area, lower calcination temperatures, shorter time of calcination, control of the stoichiometry and homogeneous distribution of the two cations. To reach these objectives, we studied two different strategies: (a) "Ordered" precursor (where the two cations are ordered as couples (A–B)–(A–B)... at atomic scale) by synthesis of a stoichiometric bimetallic precursor, a heteronuclear complex; and (b) "Disordered" precursor (where the two cations are randomly ordered at atomic scale) by preparation of an amorphous nitrate precursor by freeze-drying. $NdCoO_3$ was selected as a model because the data on its catalytic properties were scarce in the literature [14–16,19–21], the reported surface areas were very low (see below), while its activity for combustion is among the highest in the homologous series $ACoO_3$ (A = RE metal) [15,16].

2. Experimental

2.1. Preparation of catalysts

2.1.1. Materials

The materials used for the preparation of the catalysts were: neodymium sesquioxide, Nd_2O_3 (Aldrich, 99.9%), cobalt(II)oxicarbonate, $Co(OH)CO_3$, ammonium hydroxide, NH_4OH and acetone (Panreac, reagent grade), and (((carboxymethyl)imino)bis(ethylenenitrilo)tetraacetic acid, $(HOOC-CH_2)_2N-CH_2-CH_2-N(CH_2-COOH)-CH_2-CH_2-N(CH_2-COOH)_2$, (Titriplex V, Merck, analytical grade), also known as di-ethylene-triamin-pentaacetic acid, (DTPA).

2.1.2. Synthesis from ordered precursor $Co(Nd(DTPA)).7H_2O$

An aqueous suspension (ca. 100 ml) containing neodymium sesquioxide (0.005 mol) and

DTPA (0.01 mol) was heated (ca. 80°C) while stirring until a clear solution results. Then, 0.01 mol of solid cobalt(II)carbonate was added. Once the solution became clear, the pH was adjusted to 4 by addition of a 0.1 M solution of NH_3. By dropwise addition of acetone a light blue–reddish precipitate was obtained. The resulting solid was filtered, washed with an acetone:water = 1:1 mixture and dried in air at 40°C. The isolated product, that appears amorphous to X-ray diffraction, was thermogravimetrically analyzed. The ATG results were consistent with the formula $Co(Nd(DTPA)).7H_2O$. The UV–Vis spectrum revealed the existence of two different isolated chromophores, corresponding to $(Nd(DTPA))^{2-}$ and $(Co(H_2O)_x)^{2+}$ entities. Although a complementary study by IR spectroscopy was made, the connectivity between both species could not be elucidated. This results allow to establish the occurrence of a stoichiometric network of ordered metallic ions Nd–Co–Nd–Co–... [22].

Perovskite $NdCoO_3$ was obtained by two different routes: (i) a two-step process: pretreatment at 400°C for 5h, followed by calcination at 600°C for 5h; (ii) a one-step process: treatment at 700°C for 5h. All the heat treatments were carried out in an oxygen flow.

2.1.3. Synthesis from freeze-dried solutions

0.005 mol de neodymium sesquioxide were dissolved in 5 ml of concentrated nitric acid, and then added to a solution of 0.01 mol of cobalt(II)acetate in 25 ml of water. The pH of the resulting solution was adjusted to 4.5 by addition of dilute NH_3. Finally, droplets of the resulting reddish solution were frozen in liquid N_2 and transferred into a freeze-dryer operated at a pressure of 7.6 torr (1 Torr = 1.333 Nm^{-2}). The resulting blue–pink powder was placed onto an alumina boat and pretreated at 400°C for 2h under vacuum. The "ashes" were ground and treated for 24h under a dynamic oxygen atmosphere at two temperatures: 700 or 900°C.

The catalysts will be denoted hereinafter as OP (for ordered precursor) or FD (for freeze drying) followed by the final calcination temperature. Table 1 summarizes their preparative conditions.

2.1.4. Physicochemical characterization

X-ray powder diffraction (XRD) patterns were obtained by means of a Kristalloflex 810 Siemens diffractometer, using graphite-monochromated Cu Kα radiation. The patterns for structural refinements were registered in steps of 0.02°, in the 2θ angular range 20 to 85°, with an integration time of 20 s/step. Lead nitrate was used as internal standard.

Microstructure of samples was studied with a Hitachi S-2500 Scanning Electron Microscope, using an acceleration potential of 20 kV, and secondary electrons were detected. The equipment allows electron dispersive X-ray (EDX) analysis for semiquantitative composition. Spectra were recorded in the energy range 0 to 12,230 eV, with an acquisition time of 300 s.

X-ray photoelectron spectra (XPS) were recorded with a Leybold–Heraeus LHS-10 spectrometer, using Mg Kα radiation from an anode operated at 20 kV and 10 mA. The pressure in the analyzer chamber was maintained below

Table 1
Preparative conditions of the catalysts

Sample	Precursor	Thermal treatment [a]
OP-600	$Co(Nd(DTPA)).7\ H_2O$	400°C, 5 h + G + 600°C, 5 h (O_2 flow)
OP-700	$Co(Nd(DTPA)).7\ H_2O$	700°C, 5 h (O_2 flow)
FD-700	freeze-dried solution	400°C, 2 h, vacuum + G + 700°C, 5 h, (O_2 flow)
FD-900	freeze-dried solution	400°C, 2 h, vacuum + G + 900°C, 5 h, (O_2 flow)

[a] G = grinding.

10^{-8} Torr. The spectra were recorded in an energy range 20 to 50 eV, accumulating up to 200 spectra. The C 1s peak at 284.6 eV was used as internal standard.

Temperature programmed reduction (TPR) experiments were performed in a system previously described [23]. Prior to the experiment, the samples (weight = 0.1 g) were loaded in a fused quartz reactor, pretreated at 130°C for 5h in a He stream, and then cooled down to 80°C under He atmosphere, and finally outgassed under vacuum at this temperature. The reduction was carried out in a H_2 flow at a heating rate of 4°/min until 525°C, while registering continuously sample weight versus temperature.

BET specific surface area (S.S.A.) was determined by nitrogen absorption at 77K, using a conventional all-glass vacuum apparatus Micromeritics ASAP 2000. All samples were pretreated in air at 300°C for 2h and then under vacuum (10^{-6} Torr) for 16h at same temperature.

2.2. Catalytic tests

The catalytic activity for isobutene oxidation was measured between 200 and 325°C in a fixed bed, flow reactor operated at near atmospheric pressure, using a reacting mixture isobutene–oxygen–water–helium in mol ratio 1:4:1:4 and a reciprocal of space velocity (W/F) of 15 g.h/mol C_4. Experimental details were the same as those described in [24]. Briefly, catalyst was diluted with SiC tips to avoid hot spots by favouring heat transfer through the catalytic bed. SiC tips were used to fill the void space before and after the bed to avoid non-catalytic reactions. The reactor was heated to the reaction temperature in a He flow before admitting the reactants at that temperature. In these conditions, reaction in the absence of catalyst was negligible. Reactants and products were analyzed on-line gas chromatography, using two packed columns: 13X molecular sieve for O_2 and CO, and Porapak for the rest. Catalytic activity was expressed as specific rate, i.e., mol of transformed isobutene per gram of catalyst and unit time (mol/g.h). The intrinsic activity was expressed as mol of transformed isobutene per unit of catalyst surface area and unit time, i.e. mol/m^2.h. In every experiment mass and carbon balances were within 100 ± 5%.

3. Results and discussion

3.1. Bulk and surface characterization

Fig. 1 shows the XRD patterns of the catalysts precursors after calcination at different temperatures. As can be seen, the perovskite phase was already formed from both types of precursors after calcining at only 400°C, although at this temperature the single oxides of the constituting cations were also present. Nevertheless, the perovskite $NdCoO_3$ was the unique phase present in all catalyst samples: the number of peaks and their position was identical in all diffractograms, with the only difference of being much narrower and sharper for the pattern of FD-900 sample. The XRD pattern was indexed from the peak positions of reflections in the 2θ range between 20 and 85° using the TREOR program. An orthorhombic cell was obtained and refined by a least squares fitting procedure [25] leading to the following parameters: $a = 5.3574(6)$Å, $b = 5.335(1)$Å, $c = 7.545(2)$Å, $V = 215.7(1)$Å^3. The systematic absences were consistent with the space group Pbnm. Thus, this structure corresponds to the $GdFeO_3$-type. The obtained cell parameters are in good agreement with those obtained by Liu at al. [26] for $NdCoO_3$.

Scanning electron micrographs in Fig. 2 show the strong influence of the precursor nature on the morphology and particle size of the as-prepared perovskites. Samples OP-600 and OP-700 show a spongy look, their grain size ranging from 30 to 80 nm in the first case and from 30 to 150 nm in the second one. Ashes from freeze-drying precursors exhibit a more compact aspect than the OP ones, although, in the case of

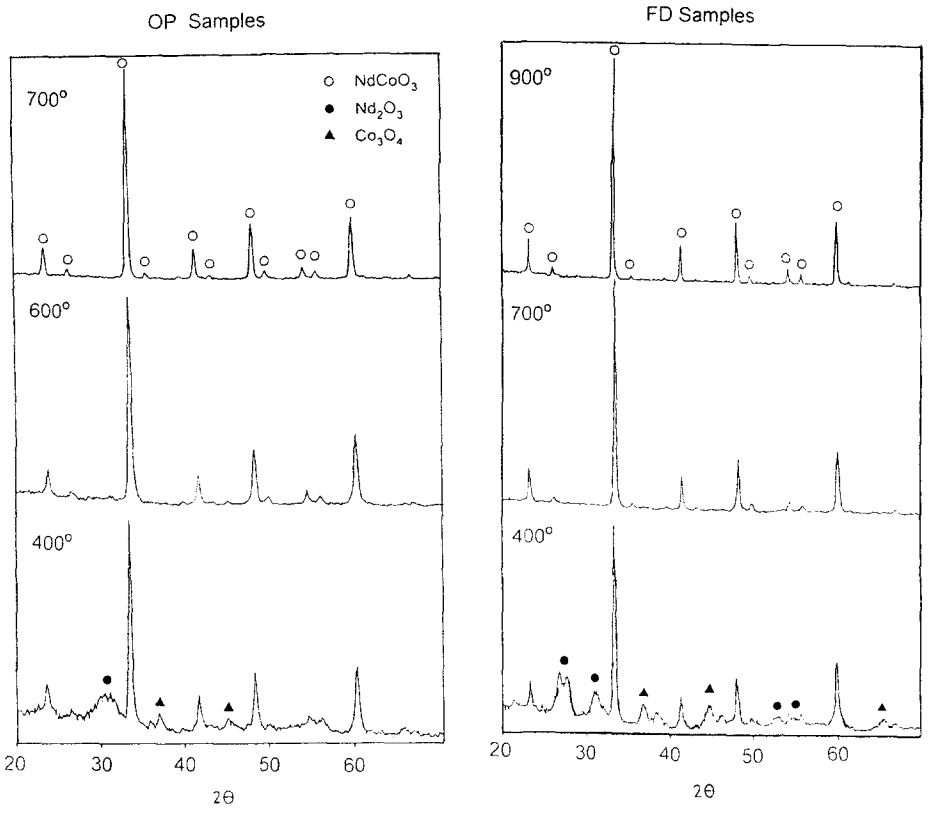

Fig. 1. XRD patterns of the OP and FD catalysts precursors after calcination at different temperatures.

sample FD-700, the grain size distribution was similar to that of sample OP-700. Finally, sample FD-900 grains were the biggest, about 600 nm, showing well-faceted, sintered particles, indicating an improvement of crystallinity. The other three samples showed rounded (non-faceted) non-sintered grains. Thus, in both sample groups the grain size increased with calcination temperature, in good agreement with the narrowing of the peaks observed in XRD patterns.

In order to study the homogeneity of the cation distribution in the grains, the composition of the surface was analyzed by two semiquantitative techniques: EDX and XPS. Results in Table 2 show that sample FD-700 surface presents a high cobalt content, enrichment that remained (although decreased) in the higher temperature sample, FD-900. On the contrary, samples OP-600 and OP-700 exhibit a Co:Nd ratio close to the theoretical stoichiometry for $NdCoO_3$. Both EDX and XPS data show a parallel trend; however, the absolute values found for FD samples by each technique are different. The origin of this difference comes from the different depth-length of "soft" X-rays in XPS and "hard" electrons in EDX: the latter analyzes a thicker layer of the grain outer surface than the former. Thus, these results allow to establish the existence of a compositional gradient from surface to the grain-core in the samples prepared from freeze-dried solutions. We found here a difference between the results of the two strategies explored: the "ordered precursor" leads to a surface composition practically stoichiometric and a uniform (gradientless) in-depth atomic composition, while the "disordered precursor" (freeze dried) leads to a

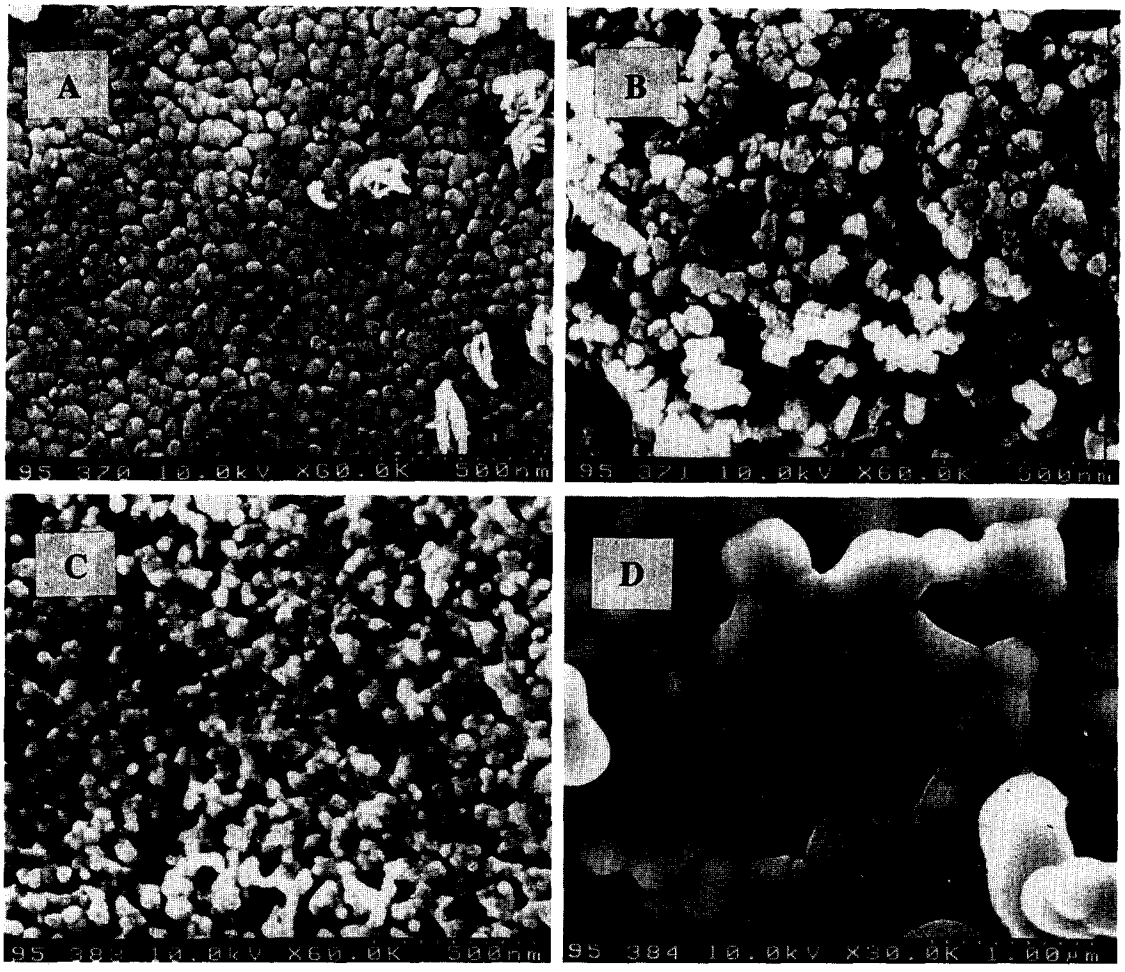

Fig. 2. Scanning electron micrograph of catalysts: (a) OP-600; (b) OP-700; (c) FD-700; and (d) FD-900.

strong surface enrichment of Co and a steep in-depth gradient of cations concentration.

Table 2 also summarizes the photoelectron binding energies (BE) corrected for charging by reference to the C 1s peak. The O 1s envelope can be resolved into two components, a low BE peak (LBE) at ca. 528 eV and a high BE (HBE) peak at ca. 531 eV. Both, LBE and HBE peaks, show similar intensities in all samples. Based on previous results of Garcia-Fierro et al. [27] the LBE peak can be ascribed to the lattice O^{2-} anion, whereas the HBE peak can be associated to the presence of hydroxyl groups chemisorbed on the surface, in agreement with the results obtained by Ichimura et al. [28], and Yamazoe et al. [29] on $LaCoO_3$ and $La_{1-x}Sr_xCoO_3$, respectively.

The Co 2p peak splitting is originated by the spin-orbit coupling of Co 2p level. The two maxima can be assigned to Co $2p_{1/2}$ the HBE at 794 eV, and to Co $2p_{3/2}$ the LBE at $\approx$ 779 eV,

Table 2
Surface composition and XPS binding energies of catalysts

Sample	Co:Nd atomic ratio		XPS B.E. (eV)		
	EDX	XPS	O 1s	Co 2p	Nd 4d
OP-600	0.96	0.96	530.6	794.4	120.5
			528.2	779.2	
OP-700	0.98	0.99	530.9	794.3	120.1
			528.5	779.3	
FD-700	1.65	2.46	530.9	795.0	121.4
			529.2	779.4	
FD-900	1.30	1.57	531.2	794.8	120.6
			528.4	779.2	

respectively. The absence of satellite peaks, characteristic of high spin Co^{2+} ions spectra, together with the occurrence of two sharp peaks, usually associated to high spin Co^{3+} ions, allows to establish that the oxidation state of surface cobalt is III [30,31]. The Nd 4d spectra show a structured broad band centered at ≈ 120.4 eV. A multiplet splitting mechanism raises the unresolved band [19]. The oxidation state of surface neodymium is Nd^{3+}.

BET specific surface areas are summarized in Table 3. As could be expected, they decrease with increasing calcination temperature in both series while, for a given calcination temperature, the freeze drying produces a higher surface area that the ordered precursor. The low value found for FD-900 is remarkable, indicating a high degree of sinterization, just as can be seen in electron micrographs.

For comparative purposes, the results previously reported in the literature are also included in Table 3. As can be seen, to our knowledge, the surface areas obtained in this work are the highest reported for the $NdCoO_3$ perovskite. Comparing similar synthetic routes, the heteronuclear complex with DTPA produced a S.S.A. fivefold higher that the use of cyanide complex [21] when calcined at the same temperature (700°C). Also the freeze dried solution of nitrates produced a S.S.A. double than the amorphous citrates [15].

Fig. 3 shows the TPR profiles from the four

Table 3
Surface areas of $NdCoO_3$ obtained by various methods

Precursor	calcination temp. (°C)	S.S.A. (m^2/g)	Ref.
$Nd_2O_3 + Co_3O_4$	1000	1.4	[19]
$Nd_2O_3 + CoO$	1300	2	[20]
Metallic nitrates	300 + 800	2.2	[14]
$Nd(Co(CN)_6).5\ H_2O$	700	1.3	[21]
Amorphous citrates	700	5.0	[15]
Mixed hydroxides	900	1.6	[16]
$Co(Nd(DTPA)).7H_2O$	600	10.8	OP-600 [a]
$Co(Nd(DTPA)).7H_2O$	700	6.7	OP-700 [a]
Freeze-dried soln.	700	12.3	FD-700 [a]
Freeze-dried soln.	900	1.6	FD-900 [a]

[a] This work.

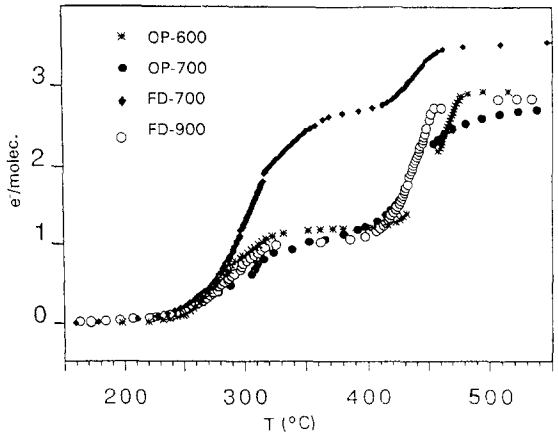

Fig. 3. TPR profiles of the catalysts. Experimental conditions in text.

samples. In all cases, the electron transferred versus temperature plots present two steps. In accordance with Baiker et al. [16] the TPR profiles of perovskites $LnCoO_3$ (Ln = La, Nd, Gd) can be interpreted based on the following scheme:

$$LnCoO_3 + H_2 \rightarrow Ln_2Co_2O_5 + H_2O \quad 1\ e^- \text{ consumption step}$$

$$Ln_2Co_2O_5 + 2\ H_2 \rightarrow Ln_2O_3 + 2Co + 2H_2O \quad 2\ e^- \text{ consumption step}$$

where the intermediate $Ln_2Co_2O_5$ adopts a perovskite-related brownmillerite-type structure.

The profiles of OP-600, OP-700 and FD-900 samples fitted to this mechanism, but that of FD-700 shows an electron consumption higher

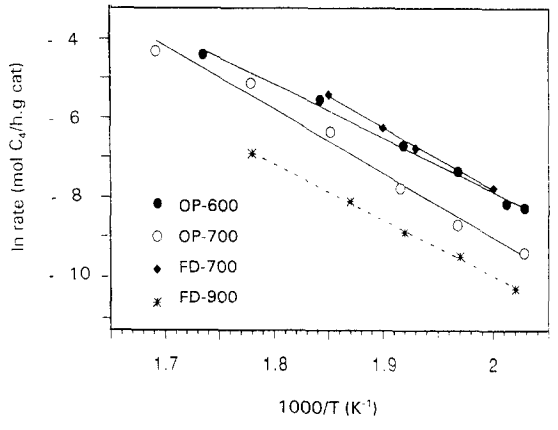

Fig. 4. Specific rates for isobutene oxidation on $NdCoO_3$ catalysts as a function of reaction temperature. Feed: isobutene–O_2–H_2O–He in mol ratio 1:4:1:4, W/F = 15 g.h/mol C_4.

than 3. This anomalous behaviour, together with the results obtained by EDX and XPS, seems to be related to the presence of cobalt-rich surface species different from $NdCoO_3$. The values of oxygen non-stoichiometry, δ, in the formula $NdCoO_{3+\delta}$, measured from these profiles was ≈ 0 for OP-600, -0.16 for OP-700, $+0.56$ for FD-700 and -0.07 for FD-900. This means that: (i) the oxygen content decreased with increasing calcination temperature in both series, leading to a slight reductive non-stoichiometry in OP-700 and FD-900; and (ii) oxidative non-stoichiometry was observed only in the sample with a high surface enrichment by Co.

3.2. Catalytic properties

It is noteworthy that, in spite of the presence of water in the feed, CO_2 was the only carbon-containing product detected in the oxidation of isobutene on every $NdCoO_3$ catalyst. Only traces of CO were found in some particular tests. Fig. 4 shows the influence of the reaction temperature on the specific rates of the different $NdCoO_3$ preparations and Table 4 summarizes some kinetic parameters. The values of apparent activation energies around 30 kcal/mol exclude the influence of diffusion phenomena in the measured rates. Within experimental error, these activation energies were the same on each sample. This indicates that the mechanism of reaction is the same for the four samples.

Ladavos and Pomonis [32] claimed that the specific total reaction rate for catalytic combustion on $La_{2-x}Sr_xNiO_{4-\lambda}$ does not seem to be influenced by the method of preparation of solids. This is not the case here, as specific rate depends on both the method and the final calcination temperature. As can be seen, the activity decreased in the order: FD-700 $\geq$ OP-600 > OP-700 > FD-900, which paralleled that of their surface areas. However, when comparing the intrinsic activity (per surface area unit) at the same temperature differences up to a 60% were found (Table 4). It may be observed that its value depended not only on the preparation method but also on the calcination temperature. If one assumes that Co surface centers are the responsible for the activity, one should expect a direct correlation between the intrinsic activity (Table 4) and the XPS surface Co content (Table 2): the higher this content is, the higher would be the number of Co surface centers per unit of catalyst surface area and, hence, the higher the intrinsic activity. However, this is not the case here as, on one hand, samples with the same XPS Co/Nd ratio show different intrinsic rates (cf. values for OP-600 and OP-700) while, on the other, those with very different Co/Nd ratio show the same intrinsic rate (cf. those of OP-700 and FD-900). Consequently, another factor should be influencing this activity parameter. The highest activity corresponds to the sample with oxidative non-stoichiometry, while the other intrinsic rate values decreased roughly with the oxygen content, i.e., with the decrease of δ. Thus, it seems that intrinsic activity depends mostly on the oxygen content of the perovskite sample.

Table 4
Surface areas and kinetic parameters of isobutene oxidation of $NdCoO_3$ catalysts

Sample	Activation energy, E_A (kcal/mol)	Specific rate [a] (mmol/h.g cat)	BET area (m^2/g)	Intrinsic activity [a] (μmol/h.m^2)
OP-600	27 ± 3	4.03	10.8	373
OP-700	32 ± 5	2.02	6.7	301
FD-700	31 ± 1	6.09	12.3	495
FD-900	29 ± 2	0.55	1.6	304

[a] At 275°C.

4. Conclusions

The use of the non-conventional methods presented here allows: (i) to obtain the highest S.S.A. reported in the literature for this particular compound; (ii) to form the perovskite structure at low temperatures (400°C); and (iii) to complete the synthesis at moderate temperatures

(600°C). Moreover, as expectable, the Ordered Precursor strategy, i.e., the synthesis of heteronuclear complexes as precursors, leads to an easier synthesis at lower temperatures as well as a perfect homogeneity in grain composition and the atomic distribution.

Nevertheless, the highest intrinsic (per surface unit) rate is shown by sample FD-700, which indicates that the increase of activity could be related to the non-stoichiometry.

Then, the procedures studied here provide a range of possibilities of preparation. The selection of a particular synthetic route to obtain a given mixed oxide structure should be made as a function of the objective of such a synthesis, either a well-crystallized, homogeneous phase or a high activity catalyst, if the activity depends mostly on the non-stoichiometry. Further work is under way to apply these strategies to the synthesis of other mixed oxides.

Acknowledgements

The financial support of the Spanish Comisión Interministerial de Investigación Científica y Técnica (CICYT) through project MAT93-0240-C04-02 is gratefully acknowledged.

References

[1] L.G. Tejuca, J.L.G. Fierro and J.M.D. Tascón, Adv. in Catal., 36 (1989) 237.
[2] N. Ramdass, Mater. Sci. Eng., 36 (1978) 231.
[3] S. Nomura, in Crystallographic and Magnetic Properties of Perovskite and Perovskite Related Oxides, Springer-Verlag, Berlin, 1978, p. 368.
[4] R.M. Hazen, Sci. American, 52 (June 1988).
[5] G. Parravano, J. Chem. Phys., 20 (1952) 342.
[6] W.F. Libby, Science, 171 (1971) 499.
[7] L.A. Pedersen and W.F. Libby, Science, 176 (1972) 1355.
[8] R.J.H. Voorhoeve, in Advanced Materials in Catalysis, Academic Press, New York, 1977, p. 129.
[9] M.A. Vannice, Catal. Rev. Sci.-Eng., 14 (1976) 153.
[10] T. Seiyama, Catal. Rev. Sci.-Eng., 34 (1992) 281.
[11] T. Shimizu, Catal. Rev. Sci.-Eng., 34 (1992) 355.
[12] F.T. Wagner, G.A. Somorjai, Nature, 285 (1980) 599.
[13] F.G. Galasso, Structure, Properties and Preparation of Perovskite-Type Compounds, Pergamon Press, Oxford, 1969.
[14] T. Nitadori, T. Ichiki and M. Misono, Bull. Soc. Chem. Japan, 61 (1988) 621.
[15] M.A. Peña, PhD Thesis, University Complutense, Madrid, 1991.
[16] A. Baiker, P.E. Marti, P. Kausch, E. Fritsch and A. Reller, J. Catalysis, 146 (1994) 268.
[17] R.H.J. Voorhoeve, J.P. Remeika, D.W. Jhonson Jr., Science, 180 (1977) 62.
[18] D. Beltrán-Porter, E. Martinez-Tamayo, R. Ibañez, A. Beltrán-Porter, J.V. Folgado, E. Escrivá, V. Muñoz, A. Segura and J. Martinez-Pastor, Solid State Ionics, 32/33 (1989) 1160.
[19] W.L. Joly, Coord. Chem. Reviews, 13 (1974) 4781.
[20] T. Arakawa, A. Yoshida and J. Siokawa, Mat. Res. Bull., 15 (1980) 347.
[21] O. Parkash, P. Ganguly, G. Rama Rao, D.S. Rajoria and V.G. Bhide, Mat. Res. Bull., 9 (1974) 1173.
[22] A. Gonzalez, Ph D. Thesis, University of Valencia, 1992.
[23] G.T. Baronetti, O.A. Scelza, A.A. Castro, V. Cortés Corberán and J.L.G. Fierro, Applied Catal., 61 (1990) 311.
[24] V. Cortés Corberán, A. Corma and G. Kremenic, Ind. & Engng. Chem., Prod. Res. Dev., 23 (1984) 546.
[25] R.G. Garvey, Least Squares Unit Cell Refinement with Indexing on the Personal Computer, Microcomputers in X-ray Diffraction, 1985.
[26] X. Liu and C.T. Prewitt, J. Phys. Chem. Solids, 52 (1991) 441.
[27] J.L. Garcia-Fierro and L.G. Tejuca, Appl. Surf. Science, 27 (1987) 453.
[28] K. Ichimura Y. Inoue and I. Yasumori, Bull. Chem. Soc. Japan, 53 (1980) 3044.
[29] N. Yamazoe, Y. Teraoka and T. Seijama, Chem. Lett., (1981) 1767.
[30] K. Ichimura, Y. Inoue and I. Yasumori, Bull. Chem. Soc. Japan, 55 (1982) 2313.
[31] A.E. Bocquet, P. Chalker, J.F. Dobson, S. Myhraa and J.G. Thompson, Physica C, 160 (1989) 252.
[32] A.K. Ladavos and P.J. Pomonis, J. Chem. Soc. Faraday Trans., 88 (1992) 2557.